Wavelength measurement of $n = 3$ to $n = 3$ transitions in highly charged tungsten ions

J. Clementson* and P. Beiersdorfer
Lawrence Livermore National Laboratory, Livermore, California 94550, USA
(Received 16 March 2010; published 19 May 2010)

$3s_{1/2}$-$3p_{3/2}$ and $3p_{1/2}$-$3d_{3/2}$ transitions have been studied in potassiumlike W^{55+} through neonlike W^{64+} ions at the electron-beam ion trap facility in Livermore. The wavelengths of the lines have been measured in high resolution relative to well known reference lines from oxygen and nitrogen ions. Using the high-energy SuperEBIT electron-beam ion trap and an $R = 44.3$ m grazing-incidence soft-x-ray spectrometer, the lines were observed with a cryogenic charge-coupled device camera. The wavelength data for the sodiumlike and magnesiumlike tungsten lines are compared with theoretical predictions for ions along the isoelectronic sequences.

DOI: 10.1103/PhysRevA.81.052509 PACS number(s): 32.30.Rj

I. INTRODUCTION

Multielectron ions of high-Z elements are of interest in atomic structure theory [1]. Accurate modeling of these systems needs to include electron correlation and relativistic effects in addition to quantum electrodynamic (QED) corrections [2,3]. Relativistic and QED effects are strongly dependent on the nuclear charge Z, which makes highly charged heavy ions suitable for investigations of high-order QED effects [4]. However, the problem of accurately calculating the structure of highly charged ions becomes challenging as the number of electrons increases. Among many-electron systems, ions with only a few valence electrons outside the last closed shell are the simplest, and those high-Z ions isoelectronic to sodium and magnesium thus represent useful stepping stones for testing QED calculations in multielectron systems.

The $3s_{1/2}$-$3p_{3/2}$ resonance transition along the sodium isoelectronic sequence has been calculated by several authors. For instance, Ivanov and Ivanova used a model potential method and extrapolated experimental data to high-Z ions [5]. Kim and Cheng calculated the wavelengths for a few high-Z ions using Dirac-Fock wave functions [6]. Johnson *et al.* performed relativistic many-body perturbation theory (RMBPT) calculations [7] from which Seely and Wagner calculated semiempirical wavelengths [8]. Predictions were also given by Kim *et al.* after investigating relativistic electron-correlation energies [2]. Baik *et al.* performed single-configuration Dirac-Fock calculations [9], whereas Seely *et al.* calculated multiconfiguration Dirac-Fock (MCDF) wavelengths [10]. Blundell added QED corrections to RMBPT calculations and studied the resonance transition for a few selected high-Z ions [11]. Theoretical wavelengths for the resonance line of magnesiumlike spectra include results of MCDF calculations by Cheng and Johnson [12], relativistic random-phase approximation (RRPA) calculations by Shorer *et al.* [13], relativistic perturbation theory using a model potential by Ivanova *et al.* [14], MCDF calculations of Marques *et al.* [15], relativistic configuration-interaction (RCI) calculations by Chen and Cheng [16], and multiconfiguration Dirac-Hartree-Fock (MCDHF) of Zou and Froese Fischer [17].

Up to xenon ($Z = 54$), the $3s_{1/2}$-$3p_{3/2}$ line has been measured for most ions isoelectronic to sodium, but for higher Z rather few measurements are reported [10,18–23]. Experimental high-precision wavelengths for the corresponding transition in magnesiumlike high-Z ions are even less common [18,19,22]. Chen *et al.* measured the $3s_{1/2}$-$3p_{3/2}$ transition in P-like through Na-like U at the Livermore EBIT-I electron-beam ion trap and found excellent agreement with RCI calculations [24]. Recently, Gillaspy *et al.* measured the $3s_{1/2}$-$3p_{3/2}$ and the $3s_{1/2}$-$3p_{1/2}$ transitions in Na-like high-Z ions, including tungsten, together with the $3s_{1/2}$-$3p_{3/2}$ transition in Mg-like and the $3p_{1/2}$-$3d_{3/2}$ transition in Al- and Si-like ions, at the electron-beam ion trap facility at the National Institute of Standards and Technology [25]. The measured $3s_{1/2}$-$3p_{3/2}$ line positions, however, did not have the accuracies required to differentiate between theories.

In the present paper, the wavelengths of the $3s_{1/2}$-$3p_{3/2}$ and $3p_{1/2}$-$3d_{3/2}$ resonance transitions in Na-, Mg-, Al-, and Si-like W ions are measured in high resolution, together with the equivalent transitions from lower charge states down to K-like W^{55+}. The measured tungsten spectra have been analyzed using theoretical spectra calculated by using the flexible atomic code (FAC) [26]. The FAC-calculated $3s_{1/2}$-$3p_{3/2}$ wavelengths are compared with results from the general-purpose relativistic atomic structure program (GRASP2) [27,28]. The measured line positions of the sodium- and magnesiumlike resonance transitions are evaluated with calculated wavelengths from several codes, including a recent result from RCI calculations [29].

II. THEORY

The structure and spectra of calciumlike W^{54+} through fluorinelike W^{65+} ions have been calculated using FAC v.1.1.1 [26,30]. FAC is a relativistic configuration-interaction program for computation of atomic radiative and collisional processes. The one-electron wave functions are derived using a modified Dirac-Fock-Slater method. QED effects are taken into account using hydrogenic approximations for the self-energy and vacuum polarization. The Breit interaction is treated in the zero-energy limit for the exchanged photon. Continuum processes are calculated using the distorted-wave approximation. The ions have been modeled with K-shell cores. Autoionization has been included for all charge states lower than neonlike from all levels to the ground and low-lying configurations

*clementson@llnl.gov; also at Atomic Physics Division, Lund University, SE-221 00 Lund, Sweden.

TABLE I. Configuration state functions used in the FAC calculations with K-shell core. $l = 0,1,\ldots,n-1$; $l^* = s,p$; $n = 3,4,5$; $n^* = 4,5$.

F-like W^{65+}	Ne-like W^{64+}	Na-like W^{63+}	Mg-like W^{62+}
$2s^22p^5$	$2s^22p^6$	$2s^22p^6nl$	$2s^22p^63lnl$
$2s2p^6$	$2s^22p^5nl$	$2s^22p^53lnl$	$2s^22p^53l3lnl$
$2s^22p^4nl$	$2s2p^6nl$	$2s2p^63lnl$	$2s2p^63l3lnl$
$2s2p^5nl$			
$2p^6nl$			
Al-like W^{61+}	**Si-like W^{60+}**	**P-like W^{59+}**	**S-like W^{58+}**
$2s^22p^63l3lnl$	$2s^22p^63l3l3lnl$	$2s^22p^63l3l3l3l3l$	$2s^22p^63l3l3l3l3l3l$
$2s^22p^53s^23l3l$	$2s^22p^53s^23l3l3l$	$2s^22p^63l^*3l^*3l^*3ln^*l$	$2s^22p^63l^*3l^*3l^*3l^*3ln^*l$
$2s^22p^53l^*3l^*3l^*n^*l$	$2s^22p^53l^*3l^*3l^*3l^*n^*l$	$2s^22p^53s^23p^3nl$	$2s^22p^53s^23p^4nl$
$2s2p^63s^23l3l$	$2s2p^63s^23l3l3l$	$2s2p^63s^23p^3nl$	$2s2p^63s^23p^4nl$
$2s2p^63l^*3l^*3l^*n^*l$	$2s2p^63l^*3l^*3l^*3l^*n^*l$		
Cl-like W^{57+}	**Ar-like W^{56+}**	**K-like W^{55+}**	**Ca-like W^{54+}**
$2s^22p^63l3l3l3l3l3l3l$	$2s^22p^63l^*3l^*3l^*3l^*3l3l3l3l$	$2s^22p^63l^*3l^*3l^*3l^*3l3l3l3l3l$	$2s^22p^63l^*3l^*3l^*3l^*3l3l3l3l3l3l$
$2s^22p^63l^*3l^*3l^*3l^*3l^*3ln^*l$	$2s^22p^63l^*3l^*3l^*3l^*3l^*3l^*3ln^*l$	$2s^22p^63l^*3l^*3l^*3l^*3l^*3l^*3l^*3ln^*l$	$2s^22p^63l^*3l^*3l^*3l^*3l^*3l^*3l^*3l3ln^*l$
$2s^22p^53s^23p^5nl$	$2s^22p^53s^23p^6nl$	$2s^22p^53s^23p^63dnl$	$2s^22p^53s^23p^63d^2nl$
$2s2p^63s^23p^5nl$	$2s2p^63s^23p^6nl$	$2s2p^63s^23p^63dnl$	$2s2p^63s^23p^63d^2nl$

of the daughter ion. Configuration state functions used in the FAC calculations are listed in Table I. In addition, the $\Delta n = 0$ M-shell transitions in K-like W^{55+} through Ne-like W^{64+} ions have also been calculated with GRASP2 [27,28]. GRASP is a multiconfiguration Dirac-Fock code for relativistic atomic calculations. The Breit interaction, self-energy, and vacuum polarization are added perturbatively. The program was run in the extended average level (EAL) calculation mode, where the radial wave functions are obtained from an average configuration approximation. Included configuration state functions are tabulated in Table II. The theoretical $3s_{1/2}$-$3p_{3/2}$ wavelengths from FAC and GRASP2 are compared with experimental line positions in Fig. 1. High-precision calculations of the sodiumlike $3s_{1/2}$-$3p_{3/2}$ line have been performed by Sapirstein *et al.* [29]. Here, the transition energy has been calculated by using the RCI and RMBPT codes and equals 537.51 eV, including electron-correlation energy. To this energy, corrections for mass polarization (−0.01 eV) and QED effects (−4.42 eV) have been added, resulting in a total energy of 533.08(4) eV, where the uncertainty is estimated to be mainly caused by the neglect of two-loop Lamb shifts and negative energy states. This transition energy corresponds to a wavelength of 23.258(2) Å.

TABLE II. Configuration state functions used in the GRASP2 calculations with filled K shell (Ne-like W) and L shell (Na- through K-like W).

Ne-like W^{64+}	Na-like W^{63+}	Mg-like W^{62+}	Al-like W^{61+}	Si-like W^{60+}
$2s^22p^6$	$3s$	$3s^2$	$3s^23p$	$3s^23p^2$
$2s^22p^53s$	$3p$	$3s3p$	$3s^23d$	$3s^23p3d$
$2s^22p^53p$	$3d$	$3s3d$	$3s3p^2$	$3s^23d^2$
$2s^22p^53d$			$3s3p3d$	$3s3p^3$
$2s2p^63s$				$3s3p^23d$
$2s2p^63p$				$3s3p3d^2$
$2s2p^63d$				
P-like W^{59+}	**S-like W^{58+}**	**Cl-like W^{57+}**	**Ar-like W^{56+}**	**K-like W^{55+}**
$3s^23p^3$	$3s^23p^4$	$3s^23p^5$	$3s^23p^6$	$3s^23p^63d$
$3s^23p^23d$	$3s^23p^33d$	$3s^23p^43d$	$3s^23p^53d$	$3s^23p^53d^2$
$3s3p^4$	$3s3p^5$	$3s3p^6$	$3s3p^63d$	$3s3p^63d^2$
$3s3p^33d$	$3s3p^43d$	$3s3p^53d$		

III. MEASUREMENT AND ANALYSIS

The experiment employed the SuperEBIT electron-beam ion trap at the Lawrence Livermore National Laboratory [31,32]. Tungsten was supplied to the trap using a metal vapor vacuum arc (MEVVA) injector, which injects few-times ionized tungsten into SuperEBIT. Trapped by electric and magnetic fields, the ions reached higher charge states under the bombardment by a narrow ($\leqslant 60$ μm) electron beam of energy 23.5 keV and beam currents around 55 mA.

The spectrometer employed for the measurement was a very high-resolution soft-x-ray grating spectrometer [33]. The

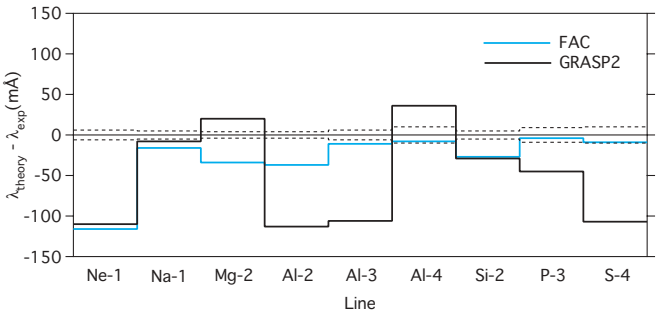

FIG. 1. (Color online) Differences between theoretical $3s_{1/2}$-$3p_{3/2}$ FAC and GRASP2 wavelengths and observed line positions in highly charged tungsten ions. Experimental uncertainties are marked with dashed lines.

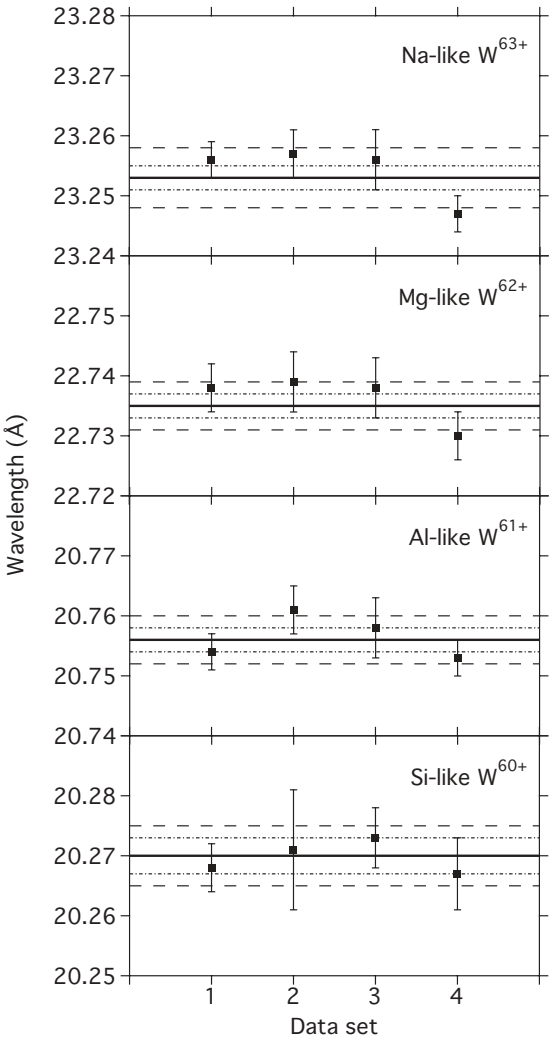

FIG. 2. Wavelengths of the Na-like through Si-like W resonance lines in the four data sets. The solid lines display the average wavelengths. Dashed lines represent the statistical and line-blend error bars, and the long-dashed lines show the final wavelength uncertainties.

instrument uses a 2400 lines/mm spherical $R = 44.3$ m grating operated at a grazing angle of 2°. The flat-field images were recorded using a cryogenically cooled Princeton Instruments charge-coupled device (CCD) detector. The back-illuminated CCD chip is made up of 1300 × 1340 pixels, each of size $20 \times 20\ \mu\text{m}^2$. The spectrometer was set up to cover the 18.5–26.5 Å soft-x-ray band. The instrument was not in best focus because of constraints placed on its use by other experiments before and after.

Nitrogen and carbon dioxide gases were supplied to the trap by a gas injector to provide accurate reference wavelengths in first order. A second-degree polynomial dispersion function of wavelength versus detector channel position was determined by using the theoretical line positions of N VII Ly-α and Ly-β, N VI $K\beta$, O VIII Ly-α, and O VII $K\alpha$ (w and z). The H-like wavelengths are taken from Garcia and Mack [34], the He-like $K\alpha$ lines from Drake [35], and the He-like $K\beta$ transition from Vainshtein and Safronova [36]. The wavelengths of the He-like ions are believed to be accurate to better than 0.6 mÅ [37]. The present measurement is thus similar to the measurement of the $2s_{1/2}$-$2p_{1/2}$ Li-like U^{89+} where the O VII lines were used as reference lines in second order [38].

Tungsten spectra were acquired during four days. The half-hour and one-hour exposure CCD images were rotated to correct for a slight tilt in the alignment of the CCD camera before the cosmic-ray and stray-light counts were filtered out, keeping only single-photon counts. The data from each day were added and analyzed separately. The $3s_{1/2}$-$3p_{3/2}$ transitions in Na- and Mg-like W and the $3p_{1/2}$-$3d_{3/2}$ in Al- and Si-like W were of sufficient strength so that they could be analyzed in each of these data sets. The wavelength dispersion determined from the nitrogen and oxygen spectra was applied to these tungsten spectra and anchored to the position of line w from He-like O VII, which showed in each spectrum, because oxygen existed in the trap as an impurity. The inferred line positions from all the data sets

TABLE III. Measured positions of the Na-like W^{63+} $3s_{1/2}$-$3p_{3/2}$ transition, error contributions, and average wavelength. Wavelengths in Å.

Data set	1	2	3	4
Wavelength	23.2556	23.2568	23.2562	23.2466
Statistics	0.0015	0.0015	0.0022	0.0016
O w statistics	0.0023	0.0036	0.0039	0.0027
Reference	0.0006			
Dispersion	0.0031			
Result		23.253 ± 0.005		

TABLE IV. Measured positions of the Mg-like W^{62+} $3s_{1/2}$-$3p_{3/2}$ transition, error contributions, and average wavelength. Wavelengths in Å.

Data set	1	2	3	4
Wavelength	22.7377	22.7391	22.7379	22.7299
Statistics	0.0016	0.0015	0.0023	0.0015
O w statistics	0.0023	0.0036	0.0039	0.0027
Line blend	0.0023	0.0026		0.0017
Reference	0.0006			
Dispersion	0.0022			
Result		22.735 ± 0.004		

TABLE V. Measured positions of the Al-like W^{61+} $3p_{1/2}$-$3d_{3/2}$ transition, error contributions, and average wavelength. Wavelengths in Å.

Data set	1	2	3	4
Wavelength	20.7544	20.7608	20.7581	20.7533
Statistics	0.0021	0.0025	0.0034	0.0021
O w statistics	0.0023	0.0036	0.0039	0.0027
Reference	0.0006			
Dispersion	0.0017			
Result		20.756 ± 0.004		

TABLE VI. Measured positions of the Si-like W^{60+} $3p_{1/2}$-$3d_{3/2}$ transition, error contributions, and average wavelength. Wavelengths in Å.

Data set	1	2	3	4
Wavelength	20.2681	20.2708	20.2730	20.2673
Statistics	0.0021	0.0029	0.0030	0.0018
O w statistics	0.0023	0.0036	0.0039	0.0027
Line blend	0.0031	0.0093		0.0049
Reference	0.0006			
Dispersion	0.0026			
Result		20.270 ± 0.005		

(see Fig. 2) were averaged to give the resulting wavelengths in Tables III, IV, V, and VI. The uncertainties in the four line positions were evaluated in each data set. The uncertainty associated with the counting statistics of each line was added to the statistical uncertainty in the O w reference-line position. The Mg- and Si-like W lines were not fully resolved, and the additional line-position uncertainties were estimated by fitting the lines separately (resonance line plus blending line) and blended (one centroid) and taking the wavelength difference as the line-blend error. These errors were added in quadrature with the statistical uncertainties. The resulting line-position uncertainties from the data sets were then averaged. To this average, the uncertainty in the theoretical reference wavelengths was added in quadrature, followed by the linear addition of the dispersion uncertainty in the calibration polynomial. The contributions to the line-position uncertainties are listed in Tables III–VI. Here, the statistical uncertainties for the lines are listed with the statistical uncertainties of the O w reference line. The reference-line error is the uncertainty of the theoretical wavelengths used for the calibration, which have been validated by measurements to agree within about 0.6 mÅ [37]. The dispersion error is the uncertainty in the linear term in the dispersion function multiplied by the distance between each line and the O w position used to anchor the dispersion.

For the weaker tungsten lines, the analysis was done after the four data sets had been summed (see Fig. 3). As with the individual data sets, the wavelength dispersion was

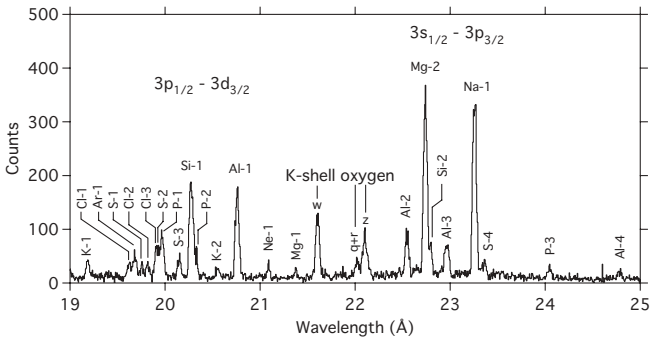

FIG. 3. Soft-x-ray spectrum of highly charged tungsten measured with an $R = 44.3$ m grazing-incidence spectrometer at the Livermore SuperEBIT electron-beam ion trap. The spectrum represents the coadded data from four run days.

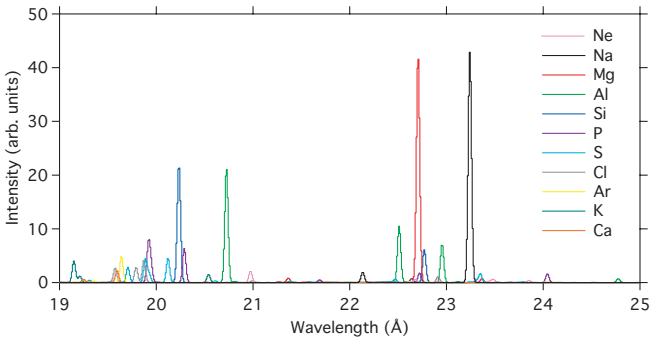

FIG. 4. (Color online) Theoretical soft-x-ray spectrum of highly charged tungsten. The spectrum is modeled with a resolution of 40 mÅ FWHM at an electron energy of 23.5 keV and a density of 5×10^{11} cm^{-3}. The charge balance is inferred from the best agreement with the spectral data in Fig. 3 and is shown in Fig. 5.

anchored to the O w line position. To identify the lines, a synthetic spectrum was calculated for an electron energy of 23.5 keV and an electron density of 5×10^{11} cm^{-3}. This spectrum is shown in Fig. 4, where the lines are modeled with an instrumental resolution of 40 mÅ full width at half maximum (FWHM). The tungsten charge balance was estimated from the measured number of counts in the observed lines and the corresponding calculated line emissivities. The resulting charge balance relative to the sodiumlike tungsten ion is shown in Fig. 5. The uncertainties in the abundances are difficult to estimate. For the ions with only a single line, the uncertainties are based on the statistics of the measured line intensities. For ions with several observed lines, the errors are estimated from both the counting statistics and the spread of the number of ions derived from each individual line. Comparison of the experimental and theoretical spectra allowed for the identification of lines from potassiumlike through neonlike tungsten. Although no calciumlike lines were observed, the abundance of Ca-like W^{54+} was set equal to that of K-like W^{55+} to account for the maximum possible influence of line blends. To estimate line-blend effects, the centroid of each line was fitted in the theoretical one-charge state spectrum and in the synthetic spectrum where lines from all ions were present. The wavelength differences were taken as the blend errors. These uncertainties were added in quadrature with the statistics of each line and O w and the reference-line

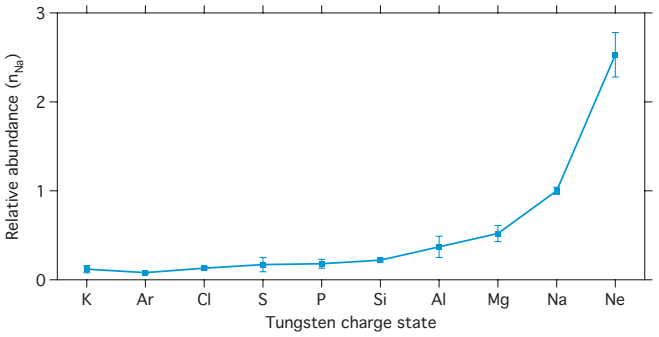

FIG. 5. (Color online) Inferred tungsten charge state distribution in SuperEBIT at an electron-beam energy of $E_b = 23.5$ keV. The charge state fractions are normalized to that of Na-like W^{63+}.

TABLE VII. Experimental and theoretical tungsten wavelengths in Å. The lines are labeled according to charge state (cf. Fig. 3). Theory from FAC, GRASP2, and RCI [29] calculations.

Key	Transition	Experiment	FAC	GRASP2	RCI
K-1	$(3s^2 3p^6 3d_{3/2})_{3/2}$-$(3s^2 3p_{1/2} 3p^4_{3/2} 3d^2_{3/2})_{3/2}$	19.184(8)	19.143	19.078	
Cl-1	$(3s^2 3p^2_{1/2} 3p^3_{3/2})_{3/2}$-$(3s^2 3p_{1/2} 3p^3_{3/2} 3d_{3/2})_{1/2}$	19.62(1)	19.570	19.442	
Ar-1	$(3s^2 3p^6)_0$-$(3s^2 3p_{1/2} 3p^4_{3/2} 3d_{3/2})_1$	19.679(7)	19.636	19.607	
S-1	$(3s^2 3p^2_{1/2} 3p^2_{3/2})_2$-$(3s^2 3p_{1/2} 3p^2_{3/2} 3d_{3/2})_1$	19.752(8)	19.702	19.592	
Cl-2	$(3s^2 3p^2_{1/2} 3p^3_{3/2})_{3/2}$-$(3s^2 3p_{1/2} 3p^3_{3/2} 3d_{3/2})_{3/2}$	19.814(9)	19.786	19.726	
Cl-3	$(3s^2 3p^2_{1/2} 3p^3_{3/2})_{3/2}$-$(3s^2 3p_{1/2} 3p^3_{3/2} 3d_{3/2})_{5/2}$		19.867	19.789	
S-2	$(3s^2 3p^2_{1/2} 3p^2_{3/2})_2$-$(3s^2 3p_{1/2} 3p^2_{3/2} 3d_{3/2})_2$		19.883	19.755	
	$(3s^2 3p^2_{1/2} 3p^2_{3/2})_0$-$(3s^2 3p_{1/2} 3p^2_{3/2} 3d_{3/2})_1$		19.922	19.852	
P-1	$(3s^2 3p^2_{1/2} 3p_{3/2})_{3/2}$-$(3s^2 3p_{1/2} 3p_{3/2} 3d_{3/2})_{3/2}$		19.916	19.789	
	$(3s^2 3p^2_{1/2} 3p_{3/2})_{3/2}$-$(3s^2 3p_{1/2} 3p_{3/2} 3d_{3/2})_{1/2}$		19.942	19.846	
S-3	$(3s^2 3p^2_{1/2} 3p^2_{3/2})_2$-$(3s^2 3p_{1/2} 3p^2_{3/2} 3d_{3/2})_3$	20.147(6)	20.116	20.006	
Si-1	$(3s^2 3p^2_{1/2})_0$-$(3s^2 3p_{1/2} 3d_{3/2})_1$	20.270(5)	20.229	20.200	
P-2	$(3s^2 3p^2_{1/2} 3p_{3/2})_{3/2}$-$(3s^2 3p_{1/2} 3p_{3/2} 3d_{3/2})_{5/2}$	20.319(5)	20.285	20.187	
K-2	$(3s^2 3p^6 3d_{3/2})_{3/2}$-$(3s^2 3p_{1/2} 3p^4_{3/2} 3d^2_{3/2})_{5/2}$	20.552(7)	20.536	20.575	
Al-1	$(3s^2 3p_{1/2})_{1/2}$-$(3s^2 3d_{3/2})_{3/2}$	20.756(4)	20.721	20.637	
Ne-1	$(2s^2 2p^2_{1/2} 2p^3_{3/2} 3s_{1/2})_1$-$(2s^2 2p^2_{1/2} 2p^3_{3/2} 3p_{3/2})_0$	21.085(6)	20.969	20.975	
Mg-1	$(3s_{1/2} 3p_{1/2})_1$-$(3s_{1/2} 3d_{3/2})_2$	21.372(6)	21.360	21.622	
Al-2	$(3s^2 3p_{1/2})_{1/2}$-$(3s_{1/2} 3p_{1/2} 3p_{3/2})_{1/2}$	22.543(4)	22.506	22.430	
Mg-2	$(3s^2)_0$-$(3s_{1/2} 3p_{3/2})_1$	22.735(4)	22.701	22.755	
Si-2	$(3s^2 3p^2_{1/2})_0$-$(3s_{1/2} 3p^2_{1/2} 3p_{3/2})_1$	22.793(5)	22.766	22.764	
Al-3	$(3s^2 3p_{1/2})_{1/2}$-$(3s_{1/2} 3p_{1/2} 3p_{3/2})_{3/2}$	22.961(6)	22.950	22.855	
Na-1	$3s_{1/2}$-$3p_{3/2}$	23.253(5)	23.237	23.245	23.258(2)
S-4	$(3s^2 3p^2_{1/2} 3p^2_{3/2})_2$-$(3s_{1/2} 3p^2_{1/2} 3p^3_{3/2})_2$	23.35(1)	23.345	23.247	
P-3	$(3s^2 3p^2_{1/2} 3p_{3/2})_{3/2}$-$(3s_{1/2} 3p^2_{1/2} 3p^2_{3/2})_{5/2}$	24.042(9)	24.038	23.997	
Al-4	$(3s^2 3p_{1/2})_{1/2}$-$(3s_{1/2} 3p_{1/2} 3p_{3/2})_{3/2}$	24.78(1)	24.770	24.814	

uncertainty, followed by a linear addition of the dispersion uncertainty. All identified lines are listed in Table VII with experimental wavelengths and theoretical line positions from FAC and GRASP2. The three lines Cl-3, S-2, and P-1 have been identified in the theoretical model. However, because the line positions overlap, a determination of these experimental wavelengths is not possible.

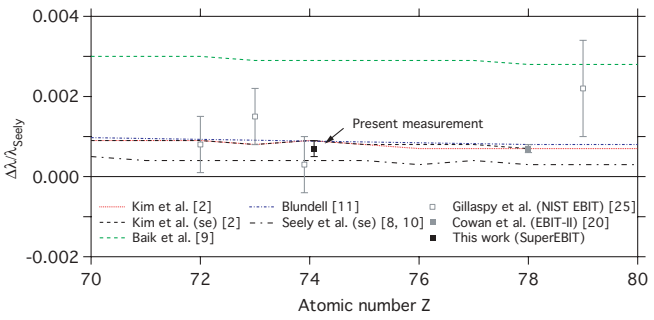

FIG. 6. (Color online) Observed $3s_{1/2}$-$3p_{3/2}$ line positions of Na-like high-Z ions [20,25] compared to theoretical line positions given by Kim *et al.* [2], Baik *et al.* [9], and Blundell [11] and to semiempirical (se) values by Kim *et al.* [2] and Seely *et al.* [8,10]. Wavelengths are normalized to the theory by Seely *et al.* [10]. Note that the wavelengths by Blundell have been interpolated. Calculations from Johnson *et al.* [7], Ivanov and Ivanova [5], and Kim and Cheng [6] are off the scale. Observed values are from measurements at the NIST EBIT [25], the Livermore EBIT-II [20], and the Livermore SuperEBIT (this work).

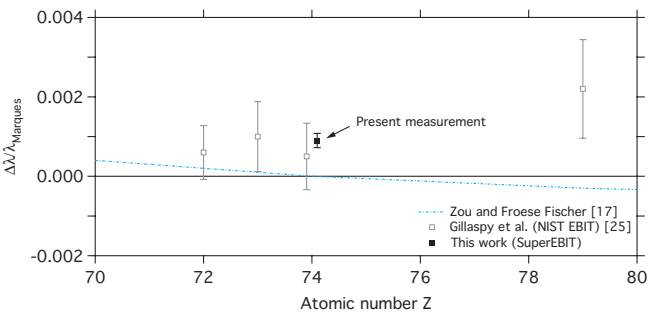

FIG. 7. (Color online) Observed $3s^2$-$3s_{1/2}3p_{3/2}$ line positions of Mg-like high-Z ions compared to theoretical line positions by Zou and Froese Fischer [17]. Wavelengths are normalized to the theory by Marques *et al.* [15]. Note that wavelengths by Zou and Froese Fischer have been interpolated. Predictions from Cheng and Johnson [12], Shorer *et al.* [13], and Ivanova *et al.* [14] are off the scale. The experimental data are from the NIST EBIT [25] and the Livermore SuperEBIT (present work).

Constants used are $hc = 12\,398.42$ Å eV $= 8065.5410$ eVcm and 1 Ry $= 13.60569$ eV.

IV. SUMMARY AND CONCLUSION

The measurement yields wavelengths for 20 soft-x-ray $\Delta n = 0$ M-shell lines in highly charged tungsten ions between 19 and 25 Å (see Table VII and Fig. 3). Lines from potassiumlike W^{55+} to neonlike W^{64+} are measured in high resolution and identified using theoretical spectra calculated using FAC (cf. Fig. 4). Comparisons with FAC and GRASP2 calculations are made for the $3s_{1/2}$-$3p_{3/2}$ transitions in K-like W^{55+} through Ne-like W^{64+} ions (see Fig. 1). The comparison shows that our FAC calculations on average do a better job in reproducing the measured values than our GRASP2 calculations. Both do poorly for the neonlike line (cf. previous work on the $2s_{1/2}$-$2p_{3/2}$ transitions in Li-like Th^{80+} and U^{82+} [39,40]). Overall, the theoretical wavelengths are too short, but not consistently.

Several calculations have been made for the resonance line in sodiumlike ions, and the observed $3s_{1/2}$-$3p_{3/2}$ tungsten line position is compared with these in Fig. 6, where sodiumlike ions with $70 \leqslant Z \leqslant 80$ are shown. The experimental wavelength of 23.253(5) Å agrees well with the *ab initio* calculations by Kim *et al.* [2], Blundell [11], and the new *ab initio* value by Sapirstein *et al.* [29]. The latter comparison is shown in Table VII. The calculations by Kim *et al.* [2] and Blundell [11] are also in good agreement with the high-precision measurement of Na-like Pt^{67+} by Cowan *et al.* [20] performed at the Livermore EBIT-II electron-beam ion trap.

A comparison between measurements and theory of the magnesiumlike resonance line displayed in Fig. 7 shows that the measured Mg-like W^{62+} wavelength of 22.735(4) does not agree with available theoretical predictions. This contrasts with the measurement by Gillaspy *et al.* [25], whose larger error bars show consistency with the two calculations. We note that the predictions from the MCDF [12], RRPA [13], and model-potential relativistic perturbation theory [14] codes are off the scale and, therefore, not shown in Fig. 7. Magnesiumlike ions are more difficult to calculate with accuracy, and additional high-precision measurements of the $3s^2$-$3s_{1/2}3p_{3/2}$ transition in high-Z ions are needed to guide theory.

ACKNOWLEDGMENTS

This work was performed under the auspices of the United States Department of Energy by Lawrence Livermore National Laboratory under Contract No. DE-AC52-07NA-27344. The authors would like to thank Todd Chambers, Miriam Frankel, Dr. Jaan Lepson, Debbie Miller, Yuri Podpaly, Ed Magee, and Professor Elmar Träbert for assistance with the measurement. The authors furthermore would like to thank Dr. K. T. Cheng, Dr. Mau Chen, and Dr. Jonathan Sapirstein for making unpublished results available. Joel Clementson would like to thank Dr. Hans Lundberg, Dr. Sven Huldt, Professor Sune Svanberg, and Professor Tomas Brage for their support.

[1] I. Martinson, Nucl. Instrum. Methods Phys. Res. B **43**, 323 (1989).
[2] Y.-K. Kim, D. H. Baik, P. Indelicato, and J. P. Deslaux, Phys. Rev. A **44**, 148 (1991).
[3] K. T. Cheng, M. H. Chen, W. R. Johnson, and J. Sapirstein, Can. J. Phys. **86**, 33 (2008).
[4] P. Beiersdorfer, J. Phys. B: At. Mol. Opt. Phys. **43**(7), 074032 (2010).
[5] L. N. Ivanov and E. P. Ivanova, At. Data Nucl. Data Tables **24**, 95 (1979).
[6] Y.-K. Kim and K.-T. Cheng, J. Opt. Soc. Am. **68**, 836 (1978).
[7] W. R. Johnson, S. A. Blundell, and J. Sapirstein, Phys. Rev. A **38**, 2699 (1988).
[8] J. F. Seely and R. A. Wagner, Phys. Rev. A **41**, 5246 (1990).
[9] D. H. Baik, Y. G. Ohr, K. S. Kim, J. M. Lee, P. Indelicato, and Y.-K. Kim, At. Data Nucl. Data Tables **47**, 177 (1991).
[10] J. F. Seely, C. M. Brown, U. Feldman, J. O. Ekberg, C. J. Keane, B. J. MacGowan, D. R. Kania, and W. E. Behring, At. Data Nucl. Data Tables **47**, 1 (1991).
[11] S. A. Blundell, Phys. Rev. A **47**, 1790 (1993).
[12] K. T. Cheng and W. R. Johnson, Phys. Rev. A **16**, 263 (1977).
[13] P. Shorer, C. D. Lin, and W. R. Johnson, Phys. Rev. A **16**, 1109 (1977).
[14] E. P. Ivanova, L. N. Ivanov, and M. A. Tsirekidze, At. Data Nucl. Data Tables **35**, 419 (1986).
[15] J. P. Marques, F. Parente, and P. Indelicato, At. Data Nucl. Data Tables **55**, 157 (1993).
[16] M. H. Chen and K. T. Cheng, Phys. Rev. A **55**, 3440 (1997).
[17] Y. Zou and C. Froese Fischer, J. Phys. B **34**, 915 (2001).
[18] J. F. Seely, U. Feldman, C. M. Brown, M. C. Richardson, D. D. Dietrich, and W. E. Behring, J. Opt. Soc. Am. B **5**, 785 (1988).
[19] E. Träbert, P. Beiersdorfer, J. K. Lepson, and H. Chen, Phys. Rev. A **68**, 042501 (2003).
[20] T. E. Cowan, C. L. Bennett, D. D. Dietrich, J. V. Bixler, C. J. Hailey, J. R. Henderson, D. A. Knapp, M. A. Levine, R. E. Marrs, and M. B. Schneider, Phys. Rev. Lett. **66**, 1150 (1991).
[21] A. Simionovici, D. D. Dietrich, R. Keville, T. Cowan, P. Beiersdorfer, M. H. Chen, and S. A. Blundell, Phys. Rev. A **48**, 3056 (1993).
[22] P. Beiersdorfer and B. J. Wargelin, Rev. Sci. Instrum. **65**, 13 (1994).
[23] P. Beiersdorfer, E. Träbert, H. Chen, M. H. Chen, M. J. May, and A. L. Osterheld, Phys. Rev. A **67**, 052103 (2003).
[24] M. H. Chen, K. T. Cheng, P. Beiersdorfer, and J. Sapirstein, Phys. Rev. A **68**, 022507 (2003).
[25] J. D. Gillaspy, I. N. Draganić, Y. Ralchenko, J. Reader, J. N. Tan, J. M. Pomeroy, and S. M. Brewer, Phys. Rev. A **80**, 010501(R) (2009).
[26] M. F. Gu, Can. J. Phys. **86**, 675 (2008).
[27] K. G. Dyall, I. P. Grant, C. T. Johnson, F. A. Parpia, and E. P. Plummer, Comput. Phys. Commun. **55**, 425 (1989).

[28] F. A. Parpia, I. P. Grant, and C. Froese Fischer (unpublished).
[29] J. Sapirstein, M. H. Chen, and K. T. Cheng (private communication).
[30] M. F. Gu, AIP Conf. Proc. **730**, 127 (2004).
[31] D. A. Knapp, R. E. Marrs, S. R. Elliott, E. W. Magee, and R. Zasadzinski, Nucl. Instrum. Methods Phys. Res. A **334**, 305 (1993).
[32] P. Beiersdorfer, Can. J. Phys. **86**, 1 (2008).
[33] P. Beiersdorfer, E. W. Magee, E. Träbert, H. Chen, J. K. Lepson, M.-F. Gu, and M. Schmidt, Rev. Sci. Instrum. **75**, 3723 (2004).
[34] J. D. Garcia and J. E. Mack, J. Opt. Soc. Am. **55**, 654 (1965).
[35] G. W. Drake, Can. J. Phys. **66**, 586 (1988).
[36] L. A. Vainshtein and U. I. Safronova, Phys. Scr. **31**, 519 (1985).
[37] L. Engström and U. Litzén, J. Phys. B **28**, 2565 (1995).
[38] P. Beiersdorfer, H. Chen, D. B. Thorn, and E. Träbert, Phys. Rev. Lett. **95**, 233003 (2005).
[39] P. Beiersdorfer, A. Osterheld, S. R. Elliott, M. H. Chen, D. Knapp, and K. Reed, Phys. Rev. A **52**, 2693 (1995).
[40] P. Beiersdorfer, D. Knapp, R. E. Marrs, S. R. Elliott, and M. H. Chen, Phys. Rev. Lett. **71**, 3939 (1993).